Energy 286 (2024) 129615

Contents lists available at ScienceDirect

Energy

journal homepage: www.elsevier.com/locate/energy

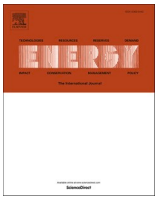

Single-step integrated CO_2 absorption and mineralization using fly ash coupled mixed amine solution: Mineralization performance and reaction kinetics

Jingwen Lu, Zhonghui Wang, Sheng Su *, Hao Liu, Zhiwei Ma, Qiangqiang Ren **, Kai Xu, Yi Wang, Song Hu, Jun Xiang

State Key Laboratory of Coal Combustion, School of Energy and Power Engineering, Huazhong University of Science and Technology, Wuhan, 430074, China

ARTICLE INFO

Handling Editor: Krzysztof (K.J.) Ptasinski

Keywords:
Fly ash
Integrated CO_2 absorption and mineralization
Mixed amine
Amine regeneration
Reaction kinetics
Mechanism

ABSTRACT

Single-step integrated CO_2 absorption and mineralization (IAM) using fly ash and mixed amine can reduce high energy consumption of absorbent regeneration while enabling the treatment of solid waste, however, the mineralization performance and kinetics are still unclear. This study adopted monoethanolamine (MEA)/N-Methyldiethanolamine (MDEA) mixed amine solution (MAS) as CO_2 absorbent and fly ash as mineralizing materials to complete the IAM process in single-step, while realizing the regeneration of mixed amine. The mineralization performance was studied, and the reaction kinetics were analyzed by surface coverage model. The results demonstrated that fly ash effectively mineralized the absorbed CO_2 in MAS and mixed amine regenerated. The mineralization efficiency reached maximum of 64.8 % at 40 °C, solid-liquid (S/L) ratio of 100 g/L, stirring rate of 500 r/min and 90 min, reaching 60.3 % after 10 cycles. The kinetic results demonstrated that surface coverage model exhibited excellent predictive capability for mineralization process (correlation coefficient (R^2) > 0.99), with identification of surface reaction governed by calcium leaching as the primary rate-limiting factor. The regeneration of mixed amine was achieved by forming carbamate and protonated amine. The CO_3^{2-}/HCO_3^- effectively reacted with the active Ca^{2+} ions in fly ash to realize mineralization, and the mineralization solid products was mainly $CaCO_3$.

1. Introduction

Post-combustion carbon capture is a promising technological for large scale CO_2 reduction from coal-fired power plants, steel plants and cement plants, of which organic amine chemical absorption is currently the most widely accepted technique for capturing CO_2 from flue gas, and it is suitable for retrofitting existing coal-fired power plants [1,2]. The organic amine chemical absorption method possesses the advantages of a rapid CO_2 absorption rate, high absorption efficiency, substantial absorption capacity and facile regeneration of the absorbent [3,4]. The technology, however, encounters some challenges such as the high energy consumption involved in CO_2 desorption and amine regeneration [5], degradation of absorbents and equipment corrosion [6], as well as the high cost in CO_2 transportation and compression and possible leakage risk of sequestered CO_2 [7]. To address these challenges, an improved CO_2 capture technology is imperative to be developed, which can effectively minimize the energy consumption of amine regeneration and mitigate the potential risk of CO_2 storage.

CO_2 mineralization as a promising carbon capture technology has received a lot of attention [8]. The exothermic reaction exhibits thermodynamic advantages, which facilitates the reduction of energy consumption and costs [9,10]. The carbonates are very stable in nature and environmental risks such as leakage can be significantly reduced [11]. Calcium-rich ores, magnesium-rich ores and alkaline solid are used to carry out carbonation reactions with CO_2. Carbon mineralization can be also applied with a variety of solid wastes, such as waste cement, fly ash, steel slag, mining tailings, etc [12,13]. Among them, fly ash, as the main solid waste from coal-fired power plants, can be used for CO_2 mineralization and has been studied extensively. By conducting CO_2 mineralization performance for fly ash at different temperature, Rao et al. [14] concluded that the promotion of mineralization reactions only occurred when the temperature exceeded 60 °C, and these reactions were

* Corresponding author. State Key Laboratory of Coal Combustion, Huazhong University of Science and Technology, Wuhan, 430074, China.
** Corresponding author.
E-mail addresses: susheng_sklcc@hotmail.com (S. Su), renqiangqiang0301@163.com (Q. Ren).

https://doi.org/10.1016/j.energy.2023.129615
Received 19 July 2023; Received in revised form 24 October 2023; Accepted 7 November 2023
Available online 9 November 2023

observed after the hydration of CaO in fly ash into $Ca(OH)_2$. The effects of temperature, gas flow rate and solid-liquid (S/L) ratio on the mineralization efficiency of fly ash were investigated Ji et al. [15]. It was observed that the mineralization efficiency remained barely affected by variations in gas flow rate and S/L ratio. Suitable additives can also be added to the process of CO_2 mineralization by fly ash to facilitate the mineralization reaction [16]. When fly ash was mixed with brine, CO_2 was sequestered in the form of carbonate, furthermore, the addition of NaOH to the mixture of fly ash and brine could enhance CO_2 sequestration [17]. However, this technology, encounters the synergistic treatment of fly ash and CO_2, faces the challenge of slow chemical reaction rates, hindering its application in industrialization [18].

Considering the advantages of fast reaction kinetics in CO_2 absorption by organic amines and low energy consumption with permanent CO_2 sequestration by CO_2 mineralization, combination of two technologies not only reduces the energy consumption of organic amine regeneration, but also promotes the mineralization reaction to generate stable products. Based on this concept, integrated CO_2 absorption and mineralization (IAM) process has been proposed and investigated [19]. Typically, two pathways are commonly employed in current research for the IAM process. One common method employed approach involves the utilization of organic amine solution for pre-absorbing CO_2, subsequently, the CO_2-rich organic amine solution is combined with the calcium-based substances to generate calcium carbonate precipitation and simultaneously realize the regeneration of the organic amine. In this pathway, the IAM process is conducted separately, so it can be called two-step process [20]. The other pathway involves establishing a mixed reaction system of calcium-based substances and organic amine solution, wherein CO_2 is continuously introduced into the system to accomplish the IAM process. This method is commonly referred to single-step process [11,21]. Some studies have utilized organic amine solutions, such as monoethanolamine (MEA), N-Methyldiethanolamine (MDEA), diethanolamine (DEA), 2-amino-2-methyl-1-propanol (AMP) and piperazine (PZ) for pre-absorption CO_2, followed by the combination with CaO, $Ca(OH)_2$ and $CaCl_2$ to facilitate CO_2 mineralization process [22–26]. It was found that the pro-absorbed CO_2 in solution could be efficiently converted into $CaCO_3$ precipitation and showed high CO_2 conversion, which verified the effectiveness of the two-step approach. Liu. et al. performed IAM process by pre-mixing CaO solids with MEA, AMP and sodium glycinate (NaGly) solutions in a slurry reaction system, resulting in exceptional CO_2 absorption-mineralization performance [11,27]. The CO_2 conversion rate exceeded 80 %, demonstrating the feasibility of the single-step approach. The advantage of the this approach over two-step approach is its ability to allow CO_2 absorption and mineralization to take place in the same unit. Additionally, both IAM reactions and organic amine regeneration can be performed at identical temperature, accelerating both reaction process while reducing the system energy consumption [11].

In exiting studies, single organic amine solutions have been widely used for IAM process [28–30], while few researches conducted the evaluation on the performance of mixed amine solution (MAS) for IAM process. In comparison to single amine solution, the mixing of different amines can enhance the limited absorption capacity of traditional amine solution, and resulting in lower energy consumption and superior recycling performance [31–33]. Thermodynamic model of system composed of CO_2 and MDEA + PZ solution was established and analyzed by Moioli and Pellegrini [34], and the findings demonstrated that PZ enhanced the CO_2 absorption rate of MDEA solution and improved its absorption capacity. The CO_2 absorption efficiency of MEA and diethylethanolamine (DEEA) solution separately mixed with N,N-dimethyl-1, 2-ethanediamine (N,N-DM12EDA), N,N-dimethyl-1,3-propanediamine (N,N-DM13PDA) and 4-amino-1-methylpiperidine (4-A1MPD), was investigated by Xiao et al. [35], founding that the addition of different amines increased CO_2 absorption load in single-amine solutions, and significantly enhanced absorption rate. However, few studies have been carried out to explore the performance of IAM process in MAS, particularly with fly ash for mineralization in single-step IAM process. In our previous studies, we conducted research on CO_2 mineralization using fly ash and CO_2 absorption using MAS were carried out [28,36]. The results demonstrated that mixed amine solution exhibited higher CO_2 absorption rate and absorption compared to single amine solution, offering an economically viable alternative by reducing the reliance on costly single amine. economy feasibility. Furthermore, its reaction rate was significantly higher than that of fly ash mineralization. Considering that water presence promoted fly ash mineralization and hydrolyzed product during mineralization facilitated mixed amine regeneration [36], therefore, the combination of mixed amine absorption and fly ash mineralization was considered as a viable approach to realize single-step IAM process. Considering the limited information available in the literatures, further investigation is required on the effects of reaction temperature, reaction times on the CO_2 absorption and mineralization performance in single-step IAM process. Additionally, the CO_2 absorption performance by mixed amine and the regeneration properties of amines in single-step IAM process are not yet clear. The mineralization reaction kinetics and mechanism of IAM process using MAS coupled with fly ash is necessary to be discovered.

In this work, a mixture solution of MEA with rapid CO_2 absorption rate and MDEA with high CO_2 absorption capacity was selected as CO_2 absorbent, while the fly ash from coal-fired boiler as the target mineralization raw material. The IAM performance was investigated in single-step process. The mechanism of CO_2 absorption-mineralization by fly ash coupled with MEA/MDEA mixed solution was analyzed using different characterization methods. Additionally, the reaction kinetics of IAM process using fly ash was studied by surface coverage model. This study will provide a scientific foundation for the single-step IAM process by fly ash coupled with MAS.

2. Experimental materials and methods

2.1. Materials

The MEA and MDEA used in the experiment were obtained from China Sinopharm Group, with purity of more than 99.7 %, which can be used without further purification. MEA/MDEA mixed solution was selected with a total organic amine concentration of 3 mol/L, containing 2 mol/L MEA and 1 mol/L MDEA, which based on the optimal proportion determined in the previous study [28]. The fly ash used in this study was collected from the outlet of an electrostatic precipitator of a coal-fired power plant in China, and its elemental composition was determined by X-ray Fluorescence spectrometer (XRF), as shown in Table 1.

2.2. IAM experimental system and process

Fig. 1 illustrated the IAM experimental system. Before the experiment, the reaction vessel was first purged by continuously passing pure CO_2 gas for 5 min to remove the internal air, 200 mL of MEA/MDEA mixed solution was then added into the slurry reaction device. In addition, a certain mass of fly ash was weighed into the solution and stirred to make them thoroughly mixed. When the slurry temperature was raised to the reaction temperature, the reaction gas (1 L/min), including CO_2 (99.99 %, $P_{CO2} = 15$ %) and N_2 (99.99 %, $P_{N2} = 85$ %) was continuously introduced into the slurry reaction device for a period of time. The reaction time, S/L ratio and stirring rate were set at 25–60 °C, 50–200 g/L and 300–900 r/min respectively. The CO_2 concentration at the reactor outlet was measured by flue gas analyzer (Gasboard-3100P, Wuhan Cubic Optoelectronics), which was used to calculate the CO_2 mass at reactor outlet.

After completion of the reaction, the product was first separated using a high-speed centrifuge, followed by filtration of the centrifuged sediment through an organic filter membrane. The filtrate and solid product were collected separately, and the CO_2 loading of filtrate was

Table 1
Elemental composition analysis of fly ash by XRF.

Oxide	SiO_2	Al_2O_3	CaO	MgO	Fe_2O_3	TiO_2	SO_3	K_2O	P_2O_5
wt/%	63.44	21.96	4.74	4.07	1.41	1.18	1.6	1.09	0.51

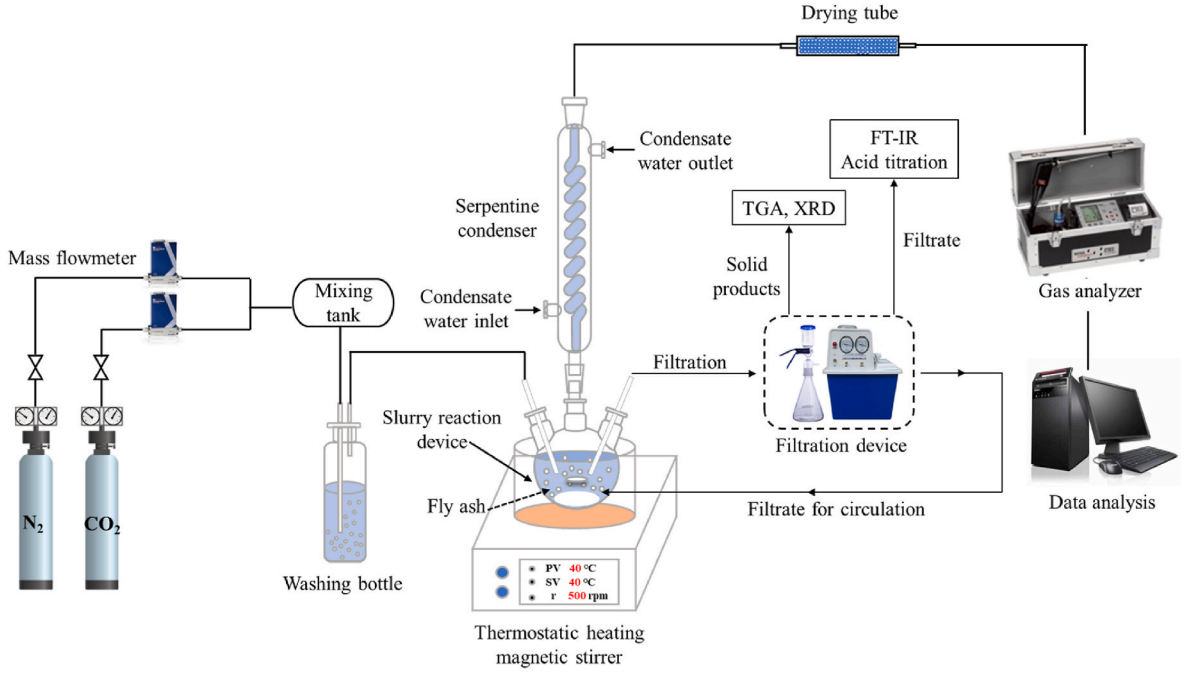

Fig. 1. IAM experimental system.

determined by acid titration. The solid product was dried at 105 °C and uniformly ground, then subjected to thermogravimetric experiments to determine the mineralization efficiency. The thermogravimetric experiments were performed on Thermogravimetric analyzer (TGA) (STA449F3, Netzsch) under the following conditions: the temperature was increased from 30 °C to 950 °C at a heating rate of 20 °C/min, and the weight change of the sample was recorded within the temperature range of 500 °C–850 °C.

Finally, the filtrates obtained from each reaction were utilized for the next IAM experiment, and the above process was repeated for 10 times, which was the cycle experiment. Since the small amount of amine solution (< 2 %) was lost during the filtration of solid product, the filtrate was supplemented with MAS of the same concentration to maintain the same S/L ratio and good experimental performance after each cycle.

2.3. Experimental methods and characterization

As shown in Table 1, the main components in the fly ash were SiO_2 and Al_2O_3, constituting over 85 % of all chemical components in fly ash. Assuming that the active components in fly ash react with CO_2 completely, the theoretical maximum CO_2 sequestration capacity can be achieved, and the theoretical maximum CO_2 sequestration capacity of fly ash could be calculated according to equation (1) [36], which was 70.6 kg-CO_2/t-FA. The mineralization efficiency in IAM experiments using fly ash was calculated as shown in the following equations [37].

$$Th\_CO_2 = \frac{44}{56} \times \left(m_{CaO} - \frac{56}{100} m_{CaCO_3} - \frac{56}{80} m_{SO_3} \right) + \frac{44}{40} m_{MgO} + \frac{44}{62} m_{Na_2O} + \frac{44}{94} m_{K_2O} \quad (1)$$

$$\eta_{CO_2} = \frac{Ac\_CO_2}{Th\_CO_2} \times 100\% \quad (2)$$

$$Ac\_CO_2 = \frac{\Delta M_{CO_2} - \Delta M'_{CO_2}}{M_{FA}} \quad (3)$$

$$\Delta M'_{CO_2} = \frac{44}{100} \times m_{CaCO_3} \times M_{FA} \quad (4)$$

where, m_{CaO} was the percentage of CaO content in fly ash, %; m_{CaCO3} was the percentage of $CaCO_3$ content in fly ash, 1.74 %; m_{SO3} was the percentage of SO_3 content in fly ash, %; m_{MgO} was the percentage of MgO content in fly ash, %; m_{Na2O} represented the percentage of Na_2O content in fly ash, %; m_{K2O} represented the percentage of K_2O content in fly ash, %. Th_CO_2 represented the theoretical CO_2 sequestration capacity, kg-CO_2/t-FA; Ac_CO_2 was the actual CO_2 sequestration capacity, kg-CO_2/t-FA; η_{CO2} was the mineralization efficiency, %; ΔM_{CO2} represented the weight change after CO_2 release by decomposition at thermogravimetric warming to 500–850 °C, kg; $\Delta M'_{CO2}$ was the mass of CO_2 released by decomposition of $CaCO_3$ in fly ash during thermogravimetric process, kg; M_{FA} was the mass of fly ash used in thermogravimetric experiments, kg.

The CO_2 mass balance between gas-liquid-solid phases was characterized by CO_2 utilization rate by equations (5)–(7):

$$\xi_{CO_2} = \left(\frac{m_{CO_2\_out} + m_{AC\_CO_2} + m_{f\_CO_2}}{m_{CO_2\_in}} \right) \times 100\% \quad (5)$$

$$m_{CO_2\_out} = 44 \times Q_v \int_0^t \frac{C_{in} - C_{out}}{22.4} dt \quad (6)$$

$$m_{AC\_CO_2} = AC\_CO_2 \times M_{tFA} \quad (7)$$

where, ξ_{CO_2} was the CO_2 utilization rate in experiments, %; $m_{CO_2\_in}$ was the CO_2 total mass at reactor inlet during the reaction, g; $m_{CO_2\_out}$ was the CO_2 total mass at reactor outlet during the reaction, g; $m_{AC\_CO_2}$ was

the mass of CO_2 involved in mineralization, g; $m_{f\_CO_2}$ was the mass of CO_2 absorbed in the filtrate after the reaction, g; Q_v was the volume of reaction gas, 1L/min; t was the reaction time, min; C_{in} and C_{out} were respectively the CO_2 concentration at reactor inlet and outlet, %; M_{tFA} was the mass of fly ash used in IAM process, kg.

The functional groups composition in the filtrate before and after the reaction were analyzed using Fourier transform infrared spectrometer (FT-IR) (EQUINOX-55, Bruker), and X-ray Diffractometer (XRD) (D8, Bruker) was used to analyze the composition and crystalline structure of the mineralization products.

2.4. Kinetic model

The surface coverage model was employed to determine CO_2 mineralization kinetic using fly ash. Assuming that the mineralization reaction process of fly ash was controlled by surface reaction, the relationship between mineralization efficiency and reaction time was shown in equations (8)–(13) [38,39].

$$\frac{d\eta_{CO_2}}{dt} = S_g M \bullet k_s \varphi \tag{8}$$

$$-\frac{d\varphi}{dt} = k_p \bullet k_s \varphi \tag{9}$$

$$k_1 = k_s S_g M \tag{10}$$

$$k_2 = k_p / S_g M \tag{11}$$

$$\varphi = \exp(-k_1 k_2 t) \tag{12}$$

$$\eta_{CO_2} = [1\text{-}\exp(-k_1 k_2 t)] / k_2 \tag{13}$$

where, S_g was the initial specific surface area of fly ash, m^2/g; M was the weight of fly ash required to consume each mole of reactive material (mainly CaO), g/mol; k_s was the rate constant, mol•min^{-1}/m^2; k_P was a proportionally constant, m^2/mol; t was reaction time, min; φ was the fraction of surface reaction sites.

3. Results and discussion

3.1. Characteristics of IAM

3.1.1. Effect of different conditions on mineralization efficiency of fly ash

The effect of temperature, S/L ratio and stirring rate on the CO_2 absorption-mineralization performance of fly ash coupled with MAS was demonstrated in Fig. 2. In Fig. 2(a), the mineralization efficiency initially increased and then gradually stabilized with the increase in reaction time at different temperatures. With the increasing of reaction temperature, the mineralization efficiency first increased and then decreased, reaching the maximum mineralization efficiency of at temperature of 40 °C. As the reaction progressed, the dissolved concentration of the active ions (Ca^{2+}, Mg^{2+}, etc.) in fly ash that could react with CO_3^{2-}/HCO_3^- to precipitate in the MAS gradually saturated and adequately reacted with the absorbed CO_2 to form carbonate precipitate, resulting in an initial increase followed by gradual stabilization in mineralization efficiency. Previous researches demonstrated that

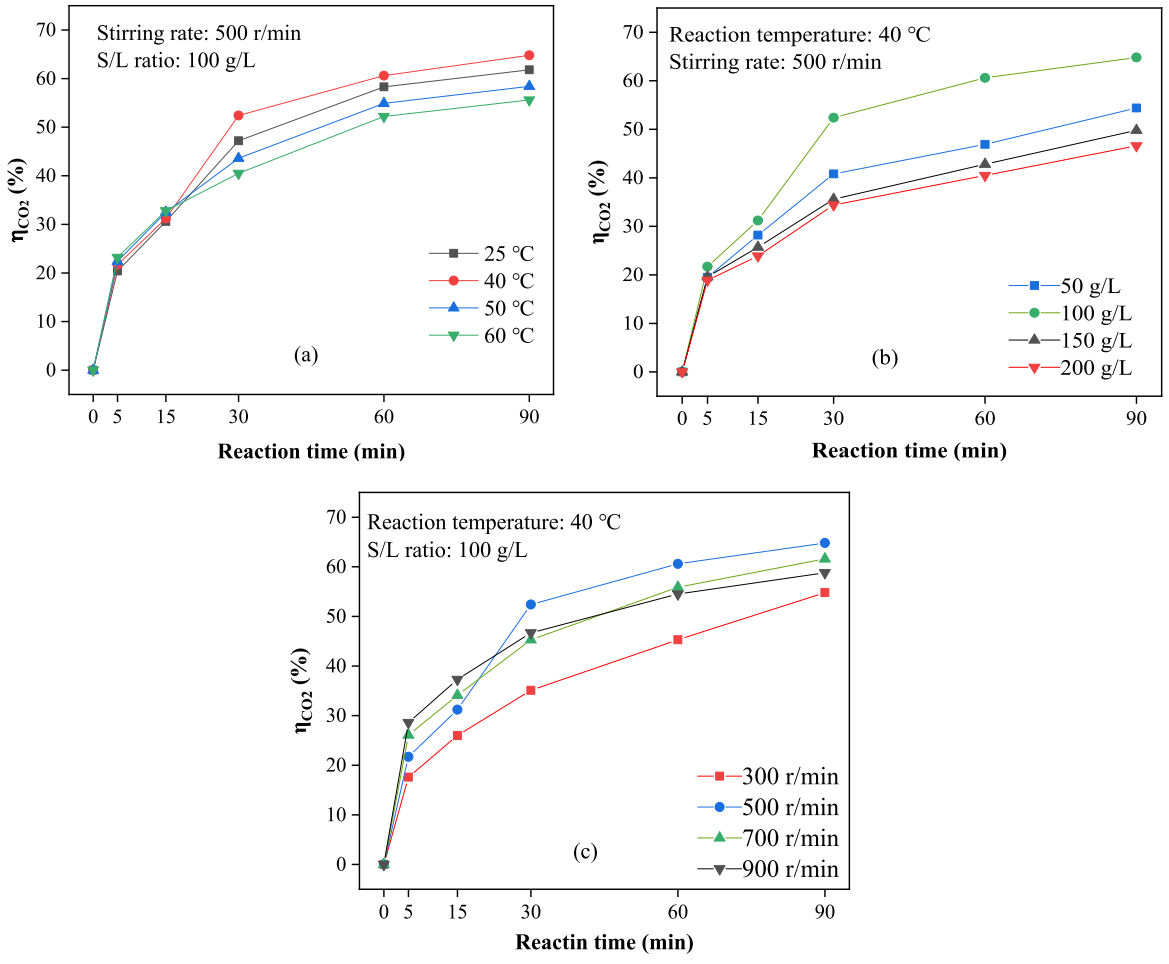

Fig. 2. CO_2 absorption-mineralization performance at (a) different temperatures, (b) different S/L ratios, (c) different stirring rates.

elevated temperature could enhance the mass transfer rate and molecular thermal motion [40], thereby facilitating the leaching and diffusion of active ions in solution as well as the diffusion of CO_2, which expediting the mineralization reaction. At 40 °C, the solubility and mass transfer rate of CO_2 in MAS made the most CO_2 to participate in reaction, which was conducive to the production of carbonate precipitate. However, the solubility of CO_2 decreased with the further increase in temperature, leading to a reduction in concentration of CO_3^{2-}/HCO_3^- in solution, which was unfavorable for the mineralization reaction and consequently led to a decline in mineralization efficiency. These findings were consistent with previous literature on the impact of temperature [41].

Fig. 2(b) showed the effect of S/L ratio on CO_2 absorption-mineralization performance of fly ash coupled with MAS at 40 °C and stirring rate of 500 r/min. It was observed that as reaction progressed, the mineralization efficiency of fly ash gradually enhanced and tended to be stable at different S/L ratios. Furthermore, the mineralization efficiency of fly ash increased first and then decreased with the S/L ratio increased from 50 g/L to 200 g/L. The maximum mineralization efficiency was achieved at S/L ratio of 100 g/L. At low S/L ratios, the reactive ions involved in the reaction in fly ash were less leached in solution. Increasing the S/L ratio enhanced dissolution rate and solubility of Ca^{2+}, Mg^{2+} and OH^- ions, promoting mineralization reactions. However, as S/L ratio further increased, the concentration of active ions dissolved in solution gradually approached saturation. Consequently, there was a limitation on leaching of active ions from fly ash to MAS, resulting in a slowdown of dissolution rate, hindering the solid-liquid mass transfer and mineralization reactions, which was consistent with existing literature [42]. Meanwhile, most of active ions dissolved in the solution participated in mineralization reaction and converted into carbonate precipitates, which covered the unreacted fly ash surface, hindering the leaching and diffusion of the remaining active ions in fly ash, resulting in lower mineralization efficiency.

The effects of stirring rate on the performance of fly ash absorption-mineralization of CO_2 at S/L ratio of 100 g/L and 40 °C were given in Fig. 2(c). The mineralization efficiency of fly ash at different stirring rates all increased firstly and reached a stable stage as reaction continued. With the increase of stirring rate, the mineralization efficiency of fly ash initially increased and then decreased. At low stirring rate, an increase in stirring rate weakened the resistance of gas-liquid mass transfer, enhancing the mass transfer rate of CO_2 between the two phases. Simultaneously, a low concentration of active ions dissolved in the solution, and intensified stirring rates facilitated leaching and diffusion of active ion in fly ash, thereby enhancing contact frequency among reactants in solution and promoting the mineralization reaction [43]. At a stirring rate of 500 r/min, the maximum rates of CO_2 mass transfer between gas and liquid as well as maximum mineralization efficiency were observed. However, with further increase in stirring rate, disturbance within the solution became more severe, leading to reduced residence time for CO_2 during gas-liquid mass transfer along with decreased rates for both gas-liquid and solid-liquid mass transfers. This finding aligned with previous literature on excessive stirring rates impact on mineralization [44]. The reduction of CO_3^{2-} in solution for absorption and conversion weakened the mineralization reaction and reduced the mineralization efficiency. Additionally, as the reaction progressed, the generated carbonate precipitate would cover the unreacted fly ash particles, inhibiting further mineralization of fly ash, resulting in a gradual leveling off of mineralization efficiency. The maximum mineralization efficiency in experiments reached 64.8 % at 40 °C, S/L ratio of 100 g/L and stirring rate of 500 r/min, which

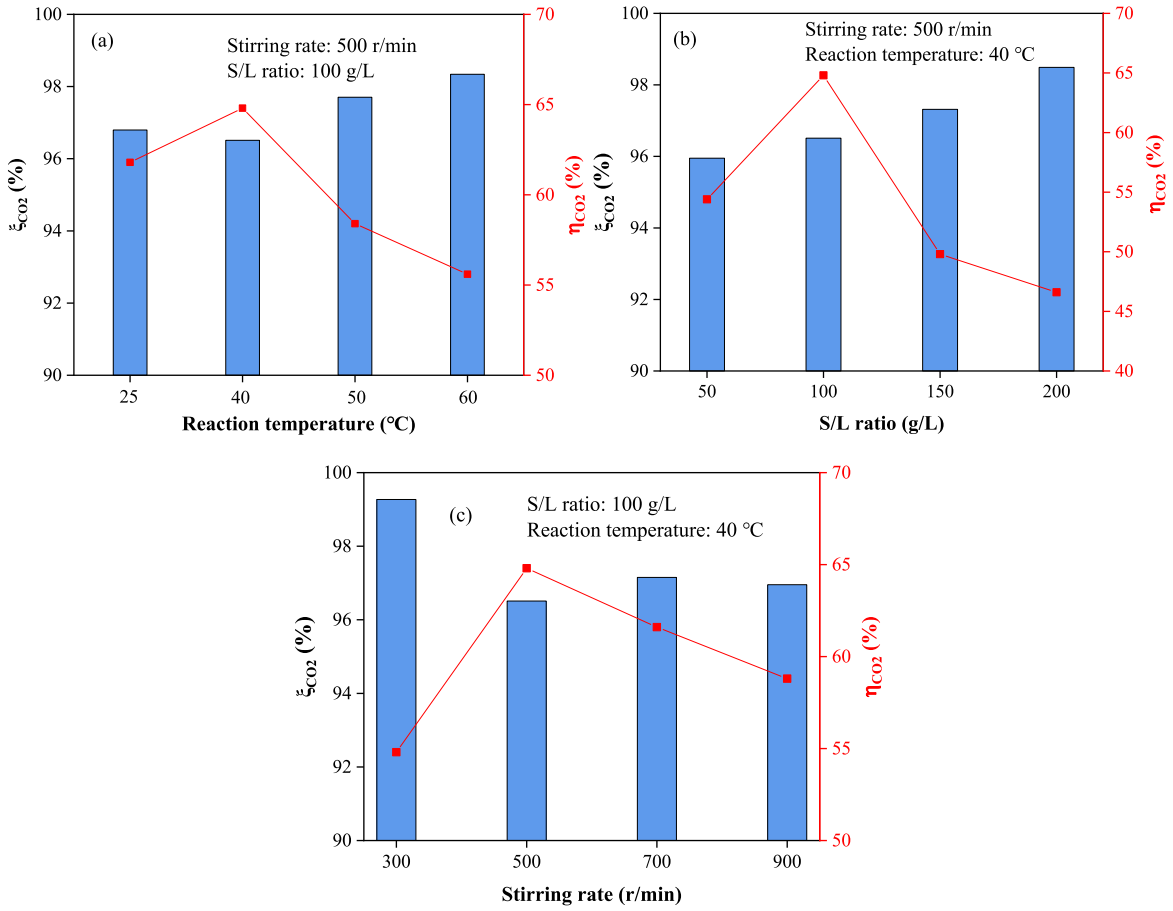

Fig. 3. Carbon balance in reactions at (a) different reaction temperature, (b) different S/L ratios, (c) different stirring rates.

represented a substantial improvement compared to exiting studies [36].

The CO_2 utilization rate in the experiments, as shown in Fig. 3, exceeded 95 %. The results indicated that the discrepancy between inlet CO_2 mass and the CO_2 mass in products did not exceed 5 % and the experimental results were credible.

3.1.2. Cyclic stability of IAM processes

The mineralization efficiency and the number of cycles played a crucial role in the cyclic stability performance of single-step IAM process by fly ash coupled with MAS. Fig. 4 illustrated the CO_2 sequestration capacity and mineralization efficiency of IAM process using fly ash during 10 cycles, at 40 °C, stirring rate of 500 r/min and S/L ratio of 100 g/L.

It can be seen the CO_2 sequestration capacity and mineralization efficiency of fly ash decreased firstly and then gradually stabilized as the number of cycles increased. The CO_2 sequestration capacity and mineralization efficiency of the second cycle exhibited a significant decrease compared with the first cycle, from 46.74 kg-CO_2/t-FA to 45.17 kg-CO_2/t-FA for CO_2 sequestration capacity and from 66.2 % to 64 % for mineralization efficiency. The CO_2 sequestration capacity and mineralization efficiency showed a gradual decline with the increasing cycle times, while the descent rate gradually reached zero. The CO_2 sequestration capacity and mineralization efficiency remained relatively stable after 7 cycles. After 10 cycles, the CO_2 sequestration capacity and mineralization efficiency of fly ash were finally stabilized at 42.6 kg-CO_2/t-FA and 60.3 % respectively, which was 91.1 % of the original MAS. The results confirmed that the absorption capacity of the MAS for CO_2 did not significantly decrease with an increase in the number of cycles. Additionally, effective regeneration was achieved, which was consistent with previous literature findings [26]. Therefore, the utilization of fly ash coupled with MAS for IAM process is a viable option, as it not only exhibits high efficiency in mineralization but also enables the recovery and utilization of MAS, thereby effectively enhancing the economy of the process.

3.2. Reaction kinetics of IAM by coupling fly ash with MAS

In order to analyze the reaction kinetics of fly ash in MAS and determine the rate-limiting steps affecting the whole reaction process, the effect of reaction temperature, S/L ratio and stirring rate on the performance of IAM using fly ash coupled MAS was investigated by surface coverage model.

The fitting results of the surface coverage model were presented in Fig. S1 and Table S1. The experimental data were found to be strongly correlated with the fitted results of the surface coverage model, with correlation coefficient (R^2) values obtained from the regressions for each reaction condition exceeding 0.99. This indicated that it was accurate and feasible using the surface coverage model to describe the absorption-mineralization reaction process of fly ash. Furthermore, the increase in reaction temperature, S/L ratio and stirring rate resulted in an initial increase and followed decrease in mineralization efficiency, which gradually stabilized with the increase of reaction time, consistent with the experimental results.

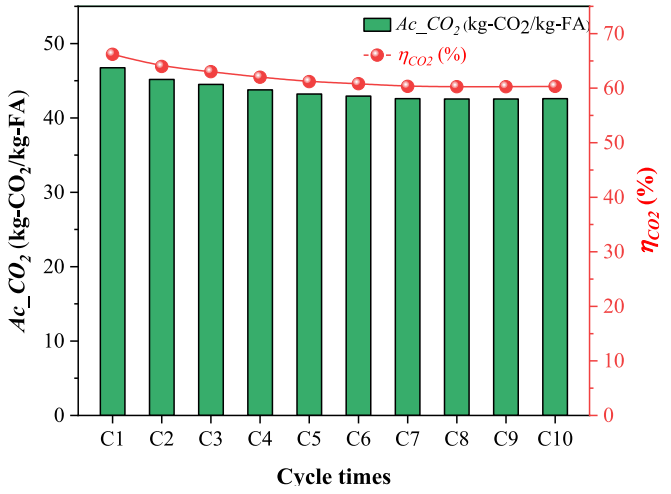

Fig. 4. Cycling performance of MAS after 10 times CO_2 absorption-mineralization experiments.

Table S1 presented the k_1 and k_2 values obtained using this model regression at different reaction conditions, and the k_s and k_p values were calculated according to equations (15) and (16). The M value and the S_g value in this experiment were 635.6 g-FA/mol-CO_2 and 9.046 m^2/g respectively. The k_s was typically affected by various factors, including the solubility and diffusion rate of CO_2 in the reaction system, the leaching rate of active ions from the solid phase to the liquid phase, and the generation rate of carbonate precipitation. Meanwhile, alternations in reaction conditions also had a significant impact on the k_s value. It can be seen from Table S1 that as reaction temperature, S/L ratio and stirring rate increased, the value of k_s initially increased and then decreased. The trend was consistent with the observed change of mineralization efficiency of fly ash. The trend of k_p was the opposite of k_s value and mineralization efficiency. The higher the value of reaction rate constant k_s, the lower the corresponding k_p value, representing a greater mineralization degree. As the reaction proceeded, the active sites on fly ash surface were gradually covered by products, hindering the leaching and diffusion of active ions from fly ash to MAS, resulting in a deceleration in reaction rate. Combining the conclusions in section 3.1, it can be concluded that the mineralization efficiency was high when the leaching rate of active ions was high in the earlier reaction period due to uncovered fly ash surface. However, as the reaction progressed and products covered the fly ash, the leaching rate of ions decreased, resulting in a reduction in mineralization efficiency. Therefore, it can be concluded that the surface reaction influenced by active ion leaching is indeed the limiting factor for fly ash mineralization.

The fitting results of surface coverage model for predicting the maximum mineralization efficiency were given in Fig. S2, which was compared with the experimentally measured values under different reaction conditions. The experimental data exhibited a strong correlation with the fitted results, showing an R^2 value was as high as 0.99 and the prediction error within ±10 %. This indicated that the surface coverage model could well describe the reaction kinetics of fly ash at different reaction conditions and accurately predict the maximum mineralization efficiency in experiments.

3.3. Mechanism analysis of the IAM processes

3.3.1. Characterization of solid products

To reveal the mechanism of IAM process using fly ash coupled MAS, XRD and TGA characterization of solid products obtained at reaction condition of 40 °C, S/L ratio of 100 g/L and stirring rate of 500 r/min were performed, as shown in Fig. 5.

It can be seen in Fig. 5(a) that the mineralogical characteristics of fly ash were complex, and the diffraction peaks representing lime (CaO) disappeared and calcite ($CaCO_3$) were significantly enhanced after the reaction, while the diffraction peaks of Portland ($Ca(OH)_2$) were not observed. It indicated that the active component CaO in fly ash reacted sufficiently with CO_2 to form calcite, which was consistent with the conclusion drawn in the literature that MEA and MDEA favored the formation of calcite [45]. The diffraction peaks of all components, except for calcite, showed no significant changes in intensity and no new diffraction peaks such as $MgCO_3$ and other carbonates were observed. This suggested that the mineralization reaction primarily occurred on CaO, while the other components in fly ash had negligible effects on IAM performance.

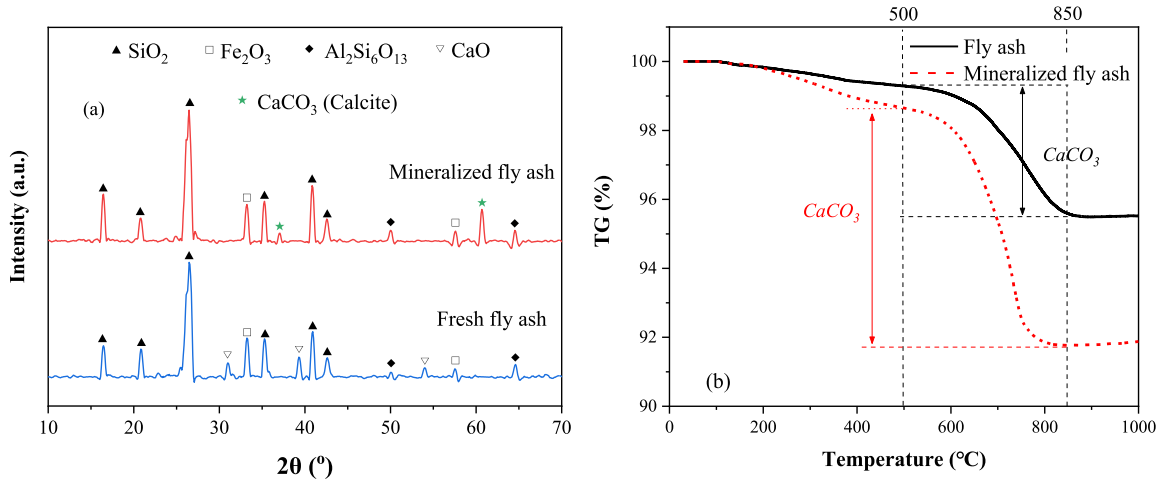

Fig. 5. (a)XRD patterns before and after the CO_2 absorption-mineralization reaction of fly ash, (b)thermogravimetric analysis before and after CO_2 absorption-mineralization reaction of fly ash.

The mass loss in the temperature range of 500–850 °C indicated the decomposition of $CaCO_3$ [46,47]. As demonstrated in Fig. 5(b), nearly all of the active CaO fraction in fly ash converted to $CaCO_3$ through reaction with CO_2, and $CaCO_3$ was the only calcium-containing carbonate phase at the end of the fly ash absorption-mineralization CO_2 reaction, consisting with the XRD analysis results.

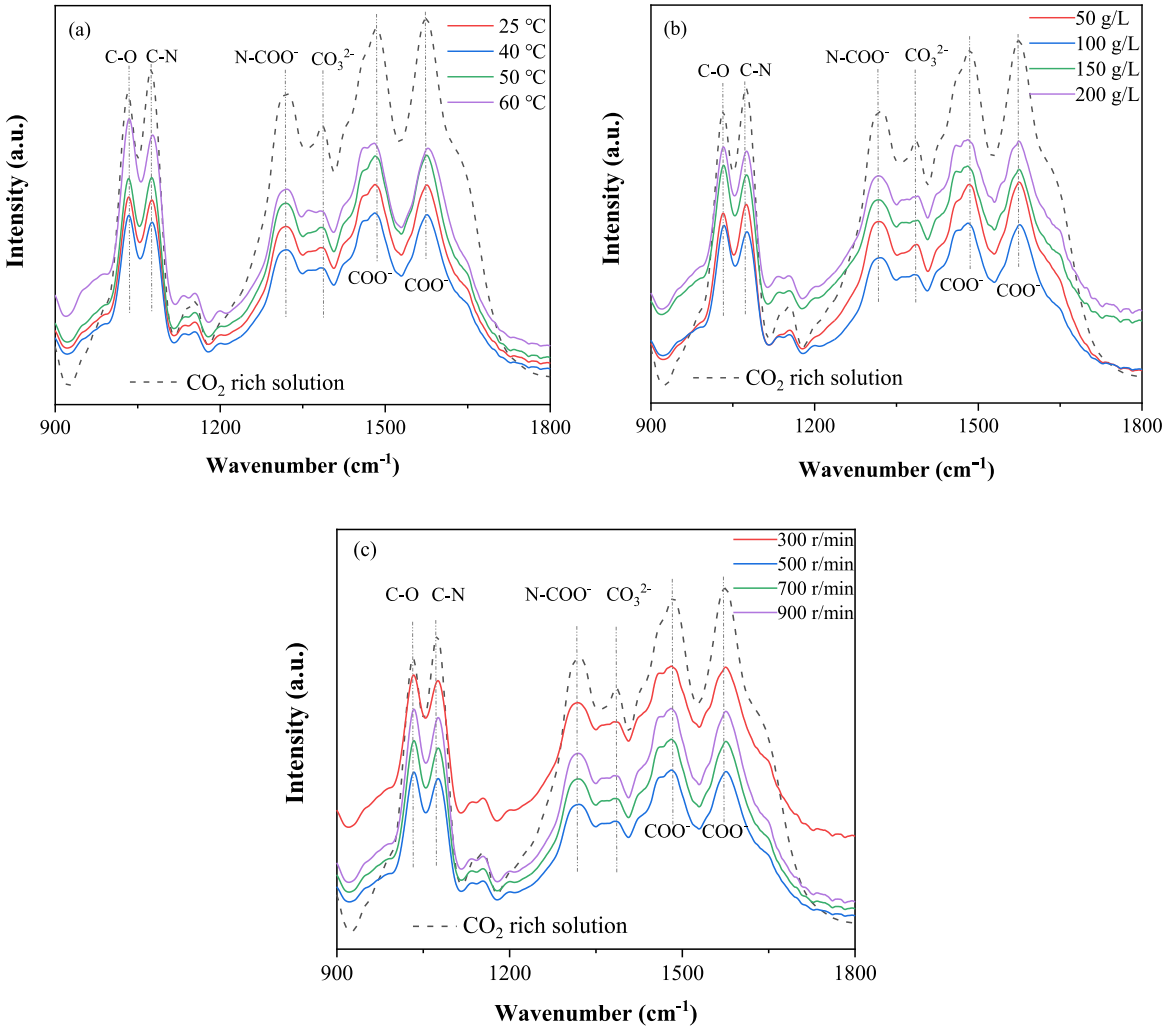

Fig. 6. FT-IR spectrums of filtrate after CO_2 absorption-mineralization reaction at (a) different reaction temperatures, (b) different S/L ratios, (c) different stirring rates.

3.3.2. Characterization of filtrate

To further reveal the mechanism of IAM process with fly ash coupled MAS, FT-IR characterization of the filtrate obtained at different reaction conditions was carried out, as shown in Fig. 6.

It can be seen that typical peaks appeared in the FT-IR spectra of the CO_2 absorption enrichment solution when the CO_2 was absorbed by the mixed amines solution, including an asymmetric stretching peak at 1568 cm^{-1}($\nu_{as}COO^-$), a symmetric stretching peak at 1486 cm^{-1} ($\nu_s COO^-$) and a stretching vibration peak appearing at 1326 cm^{-1} ($\nu NCOO^-$). The characteristic peak appearing at 1388 cm^{-1} corresponded to CO_3^{2-} and 1360 cm^{-1} to HCO_3^-. The stretching peak at 1076 cm^{-1} was attributed to C–N bond and the bending peak at 1652 cm^{-1} to the N–H bond, while the 1024 cm^{-1} corresponded to the C–O stretching peak [48,49].

It was consistent with the findings in our previous study that [28], when mixed amines reacted with CO_2, it would first react with CO_2 to form zwitterion, which would continue reacting with MEA to form carbamates and protonated amine (equation (14) and (15)), and the peak at 1568 cm^{-1}, 1486 cm^{-1} and 1326 cm^{-1} were all corresponded to the carbamate ($MEACOO^-$) produced in the reaction. The process proceeded rapidly but limited CO_2 could be absorbed. The increasing CO_2 loading facilitated the hydrolysis of carbamate to form HCO_3^- and free amines (equation (16)). Due to the absence of active hydrogen atoms surrounding the nitrogen atoms in MDEA, it did not react with CO_2 to generate carbamate directly, but involved in reaction as a weak base [26]. The peak at 1076 cm^{-1} and 1652 cm^{-1} corresponded to the protonated amine produced ($MEAH^+$/$MDEAH^+$) (equation (18)). This process proceeded relatively slow but the CO_2 absorption capacity effectively increased.

$$RNH_2 + CO_2\ (aq) \leftrightarrow RNH_2^+COO^- \tag{14}$$

$$RNH_2^+COO^- + RNH_2 \leftrightarrow RNHCOO^- + RNH_3^+ \tag{15}$$

$$RNHCOO^- + H_2O \leftrightarrow RNH_2 + HCO_3^- \tag{16}$$

$$CO_2\ (aq) + H_2O \leftrightarrow H_2CO_3 \leftrightarrow H^+ + HCO_3^- \tag{17}$$

$$R_1R_2R_3N + H^+ \rightarrow R_1R_2R_3NH^+ \tag{18}$$

The results presented in Fig. 6 demonstrated that, the peak intensities of corresponding absorption peaks in the MAS showed a decrease followed by an increase with the increase of reaction temperature, S/L ratio and stirring rate, but were all lower than those observed in the CO_2 rich solution. This trend was corresponded to the results in experiments and reaction dynamics, indicating the involvement and consumption of carbamate, CO_3^{2-}/HCO_3^- and protonated amine ($MEAH^+$/$MDEAH^+$) in the reaction. Carbamate did not participate in the CO_2 mineralization directly, however, its hydrolysis reaction provided part of HCO_3^-, which directly reacted with Ca^{2+} to form calcium carbonate precipitate and indirectly promoted the CO_2 mineralization reaction, as shown in equations (16) and (19) ~ (22).

$$CaO\ (s) + H_2O \rightarrow Ca^{2+} + 2OH^- \tag{19}$$

$$Ca^{2+} + HCO_3^- \rightarrow CaCO_3\downarrow + H^+ \tag{20}$$

$$HCO_3^- + OH^- \leftrightarrow CO_3^{2-} + H_2O \tag{21}$$

$$Ca^{2+} + CO_3^{2-} \rightarrow CaCO_3\downarrow \tag{22}$$

$$RNH_3^+ + OH^- \leftrightarrow RNH_2 + H_2O \tag{23}$$

$$R_1R_2R_3NH^+ + OH^- \leftrightarrow R_1R_2\ R_3N + H_2O \tag{24}$$

The Ca^{2+} involved in reaction primary originated from the leaching and diffusion of calcium in fly ash, which reacted directly with the CO_3^{2-}/HCO_3^- formed by the CO_2 absorption of MEA/MDEA solution to form $CaCO_3$ precipitate. Moreover, the OH^- generated from Ca^{2+} leaching also reacted directly with HCO_3^- and protonated amine ($MEAH^+$/$MDEAH^+$) (equation (19), (23) and (24)), thereby accelerating the generated protonated amine to regenerate free amine, realizing chemical regeneration of the mixed amines solution, which was in good agreement with the previous research [45]. The gradual decrease in peak intensity of $MEAH^+$ and $MDEAH^+$ proved the regeneration of the MEA/MDEA solution. The coverage of fly ash surface by the generated products resulted in a decrease in the leaching amount of Ca^{2+} and a reduction in the consumption of CO_3^{2-}/HCO_3^- in solution, as shown in Fig. 6. This observation further supported the conclusion in the reaction kinetics that the surface reaction influenced by Ca^{2+} leaching was the main factor limiting the mineralization efficiency.

3.3.3. Mechanism of IAM processes by coupling fly ash with MAS

The component of fly ash was intricate, and the active CaO component in fly ash was identified to be suitable for CO_2 mineralization and served as the primary reactant in mineralization [36]. As illustrated in Fig. 7, MEA in MAS first reacted with CO_2 to form carbamate. CO_2 was continuously introduced and reacted with water, forming H^+ and CO_3^{2-}, which resulting in a decrease in solution pH. Simultanouely, the acidic environment promoted the hydrolysis of carbamate into CO_3^{2-}, while the H^+ reacted with amine to produce protonated amine. At the same time, MDEA facilitated greater CO_2 absorption by promoting HCO_3^- generation, aligning with existing literature on this mechanism [26]. Throughout this process, Ca^{2+} leached from fly ash reacted with CO_3^{2-}/HCO_3^- to precipitate $CaCO_3$. Additionally, Additionally, OH^- generated from the hydrolysis of active CaO in fly ash reacted with protonated amine in solution to generate amine, thereby completing mineralization and amine regeneration.

4. Conclusions

Utilization of MAS coupled with fly ash on IAM process by single-step method was proposed. The mineralization efficiency increased as reaction time increased, while it initially increased and then decreased with increasing in reaction temperature, S/L ratio and stirring rate. The maximum mineralization efficiency reached 64.8 % at 40 °C, 90 min with S/L ratio of 100 g/L and stirring rate of 500 r/min. The kinetics results demonstrated that the surface coverage model exhibited excellent predictive capability for the mineralization process ($R^2 > 0.99$), with identification of Ca^{2+} leaching as the primary rate-limiting factor governing the surface reaction.

The characterization results revealed that the mineralization of fly ash was primarily attribute to active CaO in fly ash. The Ca^{2+} generated from fly ash dissolved in MEA/MDEA solution, subsequently reacting directly with CO_3^{2-}/HCO_3^- to form $CaCO_3$ precipitate. Additionally, it reacted with HCO_3^- generated through carbamate hydrolysis to facilitate the gradual recovery of carbamate into free amine. Simultaneously, the active CaO component in fly ash provided a significant amount of OH^- through hydrolysis reaction in the MEA/MDEA-H_2O system, which directly reacted with the protonated amine to regenerated the mixed amine. This work provided a new process for CO_2 absorption and mineralization using fly ash coupled MAS, contributing to the development of carbon reduction as well as fly ash utilization and treatment.

CRediT authorship contribution statement

Jingwen Lu: Conceptualization, Investigation, Writing – original draft. **Zhonghui Wang:** Conceptualization, Investigation, Writing – original draft. **Sheng Su:** Supervision, Writing – review & editing. **Hao Liu:** Supervision. **Zhiwei Ma:** Investigation, Validation. **Qiangqiang Ren:** Investigation, Writing – review & editing, Validation. **Kai Xu:** Supervision. **Yi Wang:** Supervision. **Song Hu:** Supervision. **Jun Xiang:** Supervision.

Declaration of competing interest

The authors declare that they have no known competing financial

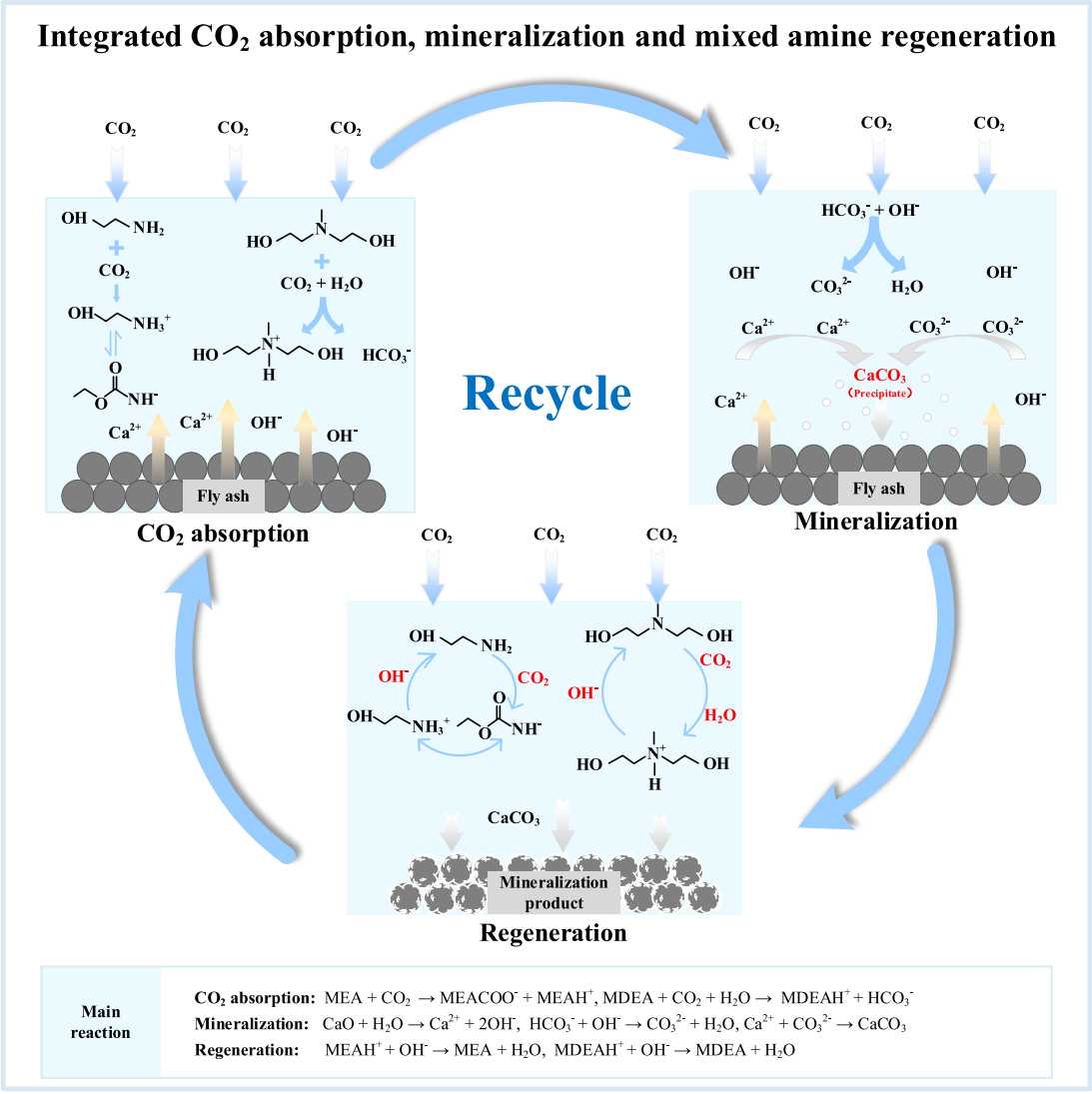

Fig. 7. Mechanism of IAM processes.

interests or personal relationships that could have appeared to influence the work reported in this paper.

Data availability

Data will be made available on request.

Acknowledgments

This work was supported by the National Key Research and Development Program of China (No. 2022YFB4202003). Also, thanks to the facility assistance from Analytical and Testing Center of Huazhong University of Science and Technology.

Appendix A. Supplementary data

Supplementary data to this article can be found online at https://doi.org/10.1016/j.energy.2023.129615.

References

[1] Perumal M, Jayaraman D, Balraj A. Experimental studies on CO_2 absorption and solvent recovery in aqueous blends of monoethanolamine and tetrabutylammonium hydroxide. Chemosphere 2021;276:130159. https://doi.org/10.1016/j.chemosphere.2021.130159.

[2] Yu Q, Wang P, Ma F, Xie HB, He N, Chen J. Computational investigation of the nitrosation mechanism of piperazine in CO_2 capture. Chemosphere 2017;186:341–9. https://doi.org/10.1016/j.chemosphere.2017.07.114.

[3] Wu Y, Xu J, Mumford K, Stevens GW, Fei W, Wang Y. Recent advances in carbon dioxide capture and utilization with amines and ionic liquids. Green Chem Eng 2020;1(1):16–32. https://doi.org/10.1016/j.gce.2020.09.005.

[4] Fu LP, Ren ZK, Si WZ, Ma QL, Huang WQ, Liao KL, Huang ZL, Wang Y, Li JH, Xu P. Research progress on CO_2 capture and utilization technology. J CO_2 Util 2022;66:102260. https://doi.org/10.1016/j.jcou.2022.102260.

[5] Li K, Leigh W, Feron P, Yu H, Tade M. Systematic study of aqueous monoethanolamine (MEA)-based CO_2 capture process: techno-economic assessment of the MEA process and its improvements. Appl Energy 2016;165:648–59. https://doi.org/10.1016/j.apenergy.2015.12.109.

[6] Zhao P, Yin Y, Xu X, Yang D, Wang J, Yang F, Zhang G. Facile fabrication of mesoporosity silica as support for solid amine CO_2 absorbents with enhanced adsorption capacity and kinetics. Energy 2022;253:124162. https://doi.org/10.1016/j.energy.2022.124162.

[7] Deng H, Bielick JM, Oppenheimer M, Fitts JP, Peters CA. Leakage risks of geologic CO_2 storage and the impacts on the global energy system and climate change mitigation. Clim Change 2017;144:151–63. https://doi.org/10.1007/s10584-017-2035-8.

[8] Pan SY, Chiang A, Chang EE, Lin YP, Kim H, Chiang PC. An innovative approach to integrated carbon mineralization and waste utilization: a review. Aerosol Air Qual Res 2015;15(3):1072–91. https://doi.org/10.4209/aaqr.2014.10.0240.

[9] Park S, Min J, Lee MG, Jo H, Park J. Characteristics of CO_2 fixation by chemical conversion to carbonate salts. Chem Eng J 2013;231:287–93. https://doi.org/10.1016/j.cej.2013.07.032.

[10] Peng N, Xiong Z, Tian C, Li HL, Zhao YC, Zhang JY, Zheng CG. Influence of carbonation under oxy-fuel combustion flue gas on the leachability of heavy metals in MSWI fly ash. Waste Manage (Tucson, Ariz) 2017;67:171–80. https://doi.org/10.1016/j.wasman.2017.05.023.
[11] Liu M, Gadikota G. Single-step, low temperature and integrated CO_2 capture and conversion using sodium glycinate to produce calcium carbonate. Fuel 2020;275:117887. https://doi.org/10.1016/j.fuel.2020.117887.
[12] Sanna A, Uibu M, Caramanna G, Kuusik R, Maroto-Valer MM. A review of mineral carbonation technologies to sequester CO_2. Chem Soc Rev 2014;43:8049–80. https://doi.org/10.1039/C4CS00035H.
[13] Chen TL, Chen YH, Dai MY, Chiang PC. Stabilization-solidification-utilization of MSWI fly ash coupling CO_2 mineralization using a high-gravity rotating packed bed. Waste Manage (Tucson, Ariz) 2021;121:412–21. https://doi.org/10.1016/j.wasman.2020.12.031.
[14] Rao A, Anthony EJ, Jia L, Macchi A. Carbonation of FBC ash by sonochemical treatment. Fuel 2007;86(16):2603–15. https://doi.org/10.1016/j.fuel.2007.02.004.
[15] Ji L, Yu H, Wang X, Grigore M, French D, Gözükara YM, Yu J, Zeng M. CO_2 sequestration by direct mineralisation using fly ash from Chinese Shenfu coal. Fuel Process Technol 2017;156:429–37. https://doi.org/10.1016/j.fuproc.2016.10.004.
[16] Liu Q, Maroto-Valer MM. Experimental studies on mineral sequestration of CO_2 with buffer solution and fly ash in brines. Energy Proc 2013;37:5870–4. https://doi.org/10.1016/j.egypro.2013.06.511.
[17] Soong Y, Fauth DL, Howard BH, Jones JR, Harrison DK, Goodman AL, Gray ML, Frommell EA. CO_2 sequestration with brine solution and fly ashes. Energy Convers Manag 2006;47(13–14):1676–85. https://doi.org/10.1016/j.enconman.2005.10.021.
[18] Huang Y, Zheng X, Wei Y, He Q, Yan S, Ji L. Protonated amines mediated CO_2 mineralization of coal fly ash and polymorph selection of $CaCO_3$. Chem Eng J 2022;450(Part 2):138121. https://doi.org/10.1016/j.cej.2022.138121.
[19] Ji L, Yu H, Yu B, Jiang K, Grigore M, Wang X, Zhao S, Li KK. Integrated absorption–mineralisation for energy-efficient CO_2 sequestration: reaction mechanism and feasibility of using fly ash as a feedstock. Chem Eng J 2018;352:151–62. https://doi.org/10.1016/j.cej.2018.07.014.
[20] Liu M, Gadikota G. Integrated CO_2 capture, conversion, and storage to produce calcium carbonate using an amine looping strategy. Energy Fuels 2019;33(3):1722–33. https://doi.org/10.1021/acs.energyfuels.8b02803.
[21] Liu M, Hohrnshil A, Gadikota G. Integrated CO_2 capture and removal via carbon mineralization with inherent regeneration of aqueous solvents. Energy Fuels 2021;35(9):8051–68. https://doi.org/10.1021/acs.energyfuels.0c04346.
[22] Park S, Lee MG, Park J. CO_2 (carbon dioxide) fixation by applying new chemical absorption-precipitation methods. Energy 2013;59:737–42. https://doi.org/10.1016/j.energy.2013.07.057.
[23] Arti M, Kang J, Youn MH, Park KT, Kim HJ, Kang SP, Jeong SK. Effect of process parameters on the $CaCO_3$ production in the single process for carbon capture and mineralization. Kor J Chem Eng 2017;34(3):935–41. https://doi.org/10.1007/s11814-016-0340-y.
[24] Kang JM, Murnandari A, Youn MH, Lee W, Park KT, Kim YE, Kim HJ, Kang SP, Lee JH, Jeong SK. Energy-efficient chemical regeneration of AMP using calcium hydroxide for operating carbon dioxide capture process. Chem Eng J 2018;335:338–44. https://doi.org/10.1016/j.cej.2017.10.136.
[25] Zhang W, Xu Y, Wang Q. Coupled CO_2 absorption and mineralization with low-concentration monoethanolamine. Energy 2022;241:122524. https://doi.org/10.1016/j.energy.2021.122524.
[26] Ji L, Yu H, Li K, Yu B, Grigore M, Yang Q, Wang X, Chen Z, Zeng M, Zhao S. Integrated absorption-mineralization for low-energy CO_2 capture and sequestration. Appl Energy 2018;225:356–66. https://doi.org/10.1016/j.apenergy.2018.04.108.
[27] Liu M, Asgar H, Seifert S, Gadikota G. Novel aqueous amine looping approach for the direct capture, conversion and storage of CO_2 to produce magnesium carbonate. Sustain Energy Fuels 2020;4(3):1265–75. https://doi.org/10.1039/C9SE00316A.
[28] Wang Z, Su S, Ma Z, Song Y, Chen Y, Liu T, Jiang L, Wang Y, Hu S, Xiang J. Study on CO_2 absorption-mineralization characteristics of mixed amine solution coupled with CaO and key influencing factors in mineralization process. J Fuel Chem Technol 2022;50(10):1371–80. https://doi.org/10.1016/S1872-5813(22)60020-3.
[29] Vinoba M, Bhagiyalakshmi M, Grace AN, Chu DH, Nam SC, Yoon Y, Yoon SH, Jeong SK. CO_2 absorption and sequestration as various polymorphs of $CaCO_3$ using sterically hindered amine. Langmuir 2013;29(50):15655–63. https://doi.org/10.1021/la403671y.
[30] Yan Z, Wang Y, Yue H, Liu C, Zhong S, Ma K, Liao W, Tang SY, Liang B. Integrated process of monoethanolamine-based CO_2 absorption and CO_2 mineralization with SFGD slag: process simulation and life-cycle assessment of CO_2 emission. Sustainable Chem Eng 2021;9(24):8238–48. https://doi.org/10.1021/acssuschemeng.1c02278.
[31] Pasha M, Li G, Shang M, Liu S, Su Y. Mass transfer and kinetic characteristics for CO_2 absorption in microstructured reactors using an aqueous mixed amine. Sep Purif Technol 2021;274:118987. https://doi.org/10.1016/j.seppur.2021.118987.
[32] Meng F, Meng Y, Ju T, Han S, Lin L, Jiang J. Research progress of aqueous amine solution for CO_2 capture: a review. Renewable Sustainable Energy Rev 2022;168:112902. https://doi.org/10.1016/j.rser.2022.112902.
[33] Xiao M, Liu H, Idem R, Tontiwachwuthikul P, Liang Z. A study of structure-activity relationships of commercial tertiary amines for post-combustion CO_2 capture. Appl Energy 2016;184:219–29. https://doi.org/10.1016/j.apenergy.2016.10.006.
[34] Moioli S, Pellegrini LA. Modeling the methyldiethanolamine-piperazine scrubbing system for CO_2 removal: thermodynamic analysis. Front Chem Sci Eng 2016;10:162–75. https://doi.org/10.1007/s11705-016-1555-5.
[35] Xiao M, Cui D, Yang Q, Liang Z, Puxty G, Yu H, Li L, Conway W, Feron P. Role of mono- and diamines as kinetic promoters in mixed aqueous amine solution for CO_2 capture. Chem Eng Sci 2021;229:116009. https://doi.org/10.1016/j.ces.2020.116009.
[36] Liu W, Su S, Xu K, Chen Q, Xu J, Sun Z, Wang Y, Hu S, Wang X, Xue Y, Xiang J. CO_2 sequestration by direct gas-solid carbonation of fly ash with steam addition. J Clean Prod 2018;178:98–107. https://doi.org/10.1016/j.jclepro.2017.12.281.
[37] El-Naas MH, Gamal ME, Hameedi S, Mohamed AMO. CO_2 sequestration using accelerated gas-solid carbonation of pre-treated EAF steel-making bag house dust. J Environ Manag 2015;156:218–24. https://doi.org/10.1016/j.jenvman.2015.03.040.
[38] Pan SY, Chiang PC, Chen YH, Tan CS, Chang EE. Kinetics of carbonation reaction of basic oxygen furnace slags in a rotating packed bed using the surface coverage model: maximization of carbonation conversion. Appl Energy 2014;113:267–76. https://doi.org/10.1016/j.apenergy.2013.07.035.
[39] Castellote M, Andrade C, Turrillas X, Campo J, Cuello GJ. Accelerated carbonation of cement pastes in situ monitored by neutron diffraction. Cement Concr Res 2008;38(12):1365–73. https://doi.org/10.1016/j.cemconres.2008.07.002.
[40] Ji L, Yu H, Yu B, Zhang RJ, French D, Grigore M, Wang XL, Chen ZL, Zhao SF. Insights into carbonation kinetics of fly ash from Victorian Lignite for CO_2 sequestration. Energy Fuels 2018;32(4):4569–78. https://doi.org/10.1021/acs.energyfuels.7b03137.
[41] Ji L, Zhang L, Zheng X, Feng L, He QY, Wei YB, Yan SP. Simultaneous CO_2 absorption, mineralisation and carbonate crystallisation promoted by amines in a single process. J CO_2 Util 2021;51:101653. https://doi.org/10.1016/j.jcou.2021.101653.
[42] Wang Y, Song L, Ma K, Liu CJ, Tang SY, Yan Z, Yue HR, Liang B. An integrated absorption–mineralization process for CO_2 capture and sequestration: reaction mechanism, recycling stability, and energy evaluation. ASC Sustainable Chem Eng 2021;9(49):16577–87. https://doi.org/10.1021/acssuschemeng.1c04731.
[43] Zhang WF, Deng ZX, Wang QH, Li J, Qiu XF. Experimental research on chemical desorption based on CO_2-rich absorption solutions. Int J Greenh Gas Control 2021;109:103356. https://doi.org/10.1016/j.ijggc.2020.103056.
[44] Zhang WF, Li J, Wang QH, Qiu XF. Desorption and mineralization of CO_2 in amine-based solution by $Ca(OH)_2$. Int J Greenh Gas Control 2020;97:103056.
[45] Arti M, Youn MH, Park KT, Kim HJ, Kim YE, Jeong SK. Single process for CO_2 capture and mineralization in various alkanolamines using calcium chloride. Energy Fuels 2017;31(1):763–9. https://doi.org/10.1021/acs.energyfuels.6b02448.
[46] Richner G, Puxty G. Assessing the chemical speciation during CO_2 absorption by aqueous amines using in situ FTIR. Ind Eng Chem Res 2012;51(44):14317–24. https://doi.org/10.1021/ie302056f.
[47] Robinson K, McCluskey A, Attalla MI. An FTIR spectroscopic study on the effect of molecular structural variations on the CO_2 absorption characteristics of heterocyclic amines. ChemPhysChem 2011;12(6):1088–99. https://doi.org/10.1002/cphc.201001056.
[48] Chang EE, Pan SY, Chen YH, Tan CS, Chiang PC. Accelerated carbonation of steelmaking slags in a high-gravity rotating packed bed. J Hazard Mater 2012;227–228:97–106. https://doi.org/10.1016/j.jhazmat.2012.05.021.
[49] Kim T, Olek J. Effects of sample preparation and interpretation of thermogravimetric curves on calcium hydroxide in hydrated pastes and mortars. Transport Res Rec 2012;2290(1):10–8. https://doi.org/10.3141/2290-02.